TECHNICKÝ DOKUMENT ČHMÚ

DYNAMICAL PARAMETERS FOR THE NEW OPERATIONAL APPLICATION OF THE ALADIN SYSTEM AT CHMI AIMING TO USE NONHYDROSTATIC EQUATIONS AT A 2.325KM HORIZONTAL RESOLUTION

Petra Smolíková

Datum vydání:15.4.2019

1   The ALADIN System

The ALADIN System is the set of pre-processing, data assimilation, model, post-processing and verification software shared and developed by the partners of the ALADIN consortium to be used for running a high-resolution limited-area model (LAM) for producing the best possible operational Numerical Weather Prediction (NWP) applications. The ALADIN consortium is a collaboration between the National (Hydro)Meteorological Services (NHMSs) of 16 European and North-African countries. The codes of the ALADIN System are common with the codes of the global Integrated Forecast System (IFS) of the ECMWF and the global ARPEGE model of Météo-France [4], [3]. The ALADIN consortium shares its code with the HIRLAM consortium consisting of 10 European NHMSs, in a close scientific and technical collaboration. Since the ALADIN System is used not only for operational but for research purposes as well and since it is shared among many partners with different needs, it contains many pieces which may or may not be activated for a particular application. For the sake of easier referencing and simplicity, the three Canonical Model Configurations were defined in [6] and [5] referring to a set of particular choices made in the whole system: ALARO, AROME and HARMONIE-AROME. This document describes the particular choices made in the dynamics part of the ALADIN System to run effectively and successfully the operational NWP application at CHMI after the transition to higher horizontal resolution. Only relevant model parts are mentioned, many times without further explanation, while all the rest is omitted.

2   Operational application of the ALADIN System at CHMI

The operational application of the ALADIN System at CHMI is based on the ALARO Canonical Model Configuration. The ALARO CMC refers to a set of physical parameterizations simulating processes of radiation, turbulence, microphysics, convection, sedimentation, orographic gravity wave drag and surface effects in a consistent way allowing a smooth transition from the mesoscale to the convection permitting scales. The detailed description of the ALARO components may be found in [6].

The ALARO CMC may be run with two different sets of basic equations discretized in space and time which are referred to as "model dynamics". The first one is a set of hydrostatic primitive equations (HPE) and the second one is a set of the nonhydrostatic fully compressible Euler equations (NHE) as described in [2]. The transition from HPE to NHE has to be done when the size of smallest circulation structures resolved in horizontal becomes comparable to their largest vertical size and so the nonhydrostatic effects become important. This limit is placed roughly to horizontal grid point distance of 3km.

The Czech operational application, being a limited area model (LAM), gets the information from the global model ARPEGE on the lateral boundaries using the Davies relaxation scheme. The model fields are imposed with the information from the host model in the so called coupling zone.

We call "current" the operational application of CHMI which served its purposes until 5 March 2019 00UTC. This application was being run on the domain with 432x540 grid points at 4.7km horizontal distance. In vertical, the domain is discretized in 87 model levels using mass-based hybrid pressure terrain-following vertical coordinate. The model

horizontal grid is linearly truncated when going to spectral space. It means that model variables are represented by 215x269 spectral coefficients in each vertical model level. The altitude of the highest grid point in the domain is 3445m. The coupling zone covers 8 grid points in each horizontal direction.

We call "target" the operational application of CHMI which was launched for the first time on 5 March 2019 at 06UTC and is running on the domain roughly covering the same territory (see Fig. 1) while the orography is calculated with higher precision from GMTED2010 physiographic data. The domain has 864x1080 grid points at 2.325km horizontal distance, and 87 model levels are kept in vertical. Linear truncation needs 431x539 spectral coefficients for the fields representation in the spectral space. The altitude of the highest grid point in the domain is increased to 4020m representing more realistically the Alpine region. In order to keep the width of the coupling zone in distance, it was enlarged to 16 grid points in each horizontal direction.
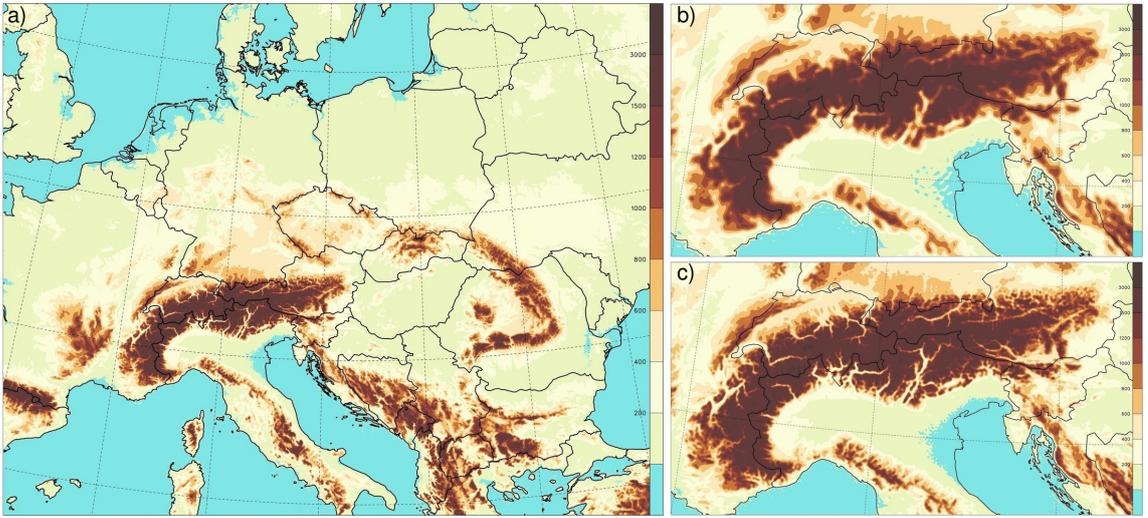

Figure 1: The target Czech operational domain orography (a) with the detail of Alps in the current (b) and the target (c) resolutions.

When going from 4.7km to 2.325km resolution we cross the imaginary limit for meaningful application of the hydrostatic hypothesis and the change from HPE to NHE is necessary. It follows that several choices have to be made in dynamical parameters to set up the nonhydrostatic dynamical core. Moreover, the change in horizontal resolution and the transition to NHE forces several other revisions in dynamics, the main being the usage of the iterative centered implicit (ICI) temporal scheme instead of the simpler extrapolating time scheme SETTLS (Stable Extrapolation Two Time Level Scheme, see [7]) in the nonlinear model part. We keep indeed the semi-Lagrangian (SL) advection. The combination of ICI and SL advection enables the usage of longer time steps while keeping reasonable stability properties. The price to be paid for the additional iterations may be reduced if semi-Lagrangian trajectories are not recomputed but are stored from the predictor step.

In Section 3, we describe the experimental setup and discuss the properties of the ICI scheme in real simulation when either single iteration or two iterations are applied. We show that the increase in the CPU time needed for a single iteration ICI scheme is only about 20% compared to SETTLS scheme when SL trajectories are not recomputed. We tune the parameters of horizontal diffusion combining two approaches: the nonlinear flow dependent grid point diffusion applied within the SL interpolations and vertically de-

pendent spectral horizontal diffusion. This approach is called SLHD (Semi-Lagrangian Horizontal Diffusion, see [8]). The aim is to get the best possible results in individual cases and the best possible objective scores for longer period runs. We discuss the results in Section 4.

In Section 5 we summarize dynamical namelists with the parameters used for the target operational application. In Section 6, we compare the results of the current operational suite (4.7km in horizontal, HPE) with the target parallel suite results (2.325km in horizontal, NHE). In Appendix, we discuss the CPU time needed for different configurations to obtain one 24 hours integration and the effectivity of the used methods.

3   Experimental environment

We choose a case of 08 June 2016 with severe convective precipitations, the forecast starts as dynamical adaptation (no data assimilation) with default DFI filter, from the ARPEGE lateral boundary conditions coupled every 3 hours. We integrate from 00UTC for 24 hours.

3.1   Reference experiments

Since the move from lower resolution to higher resolution together with the change of basic equations leading to further changes in the design of the whole application is too huge to be done in one step, we proceed gradually. First a basic nonhydrostatic setting was found and the reference experiments were run with this setting on both, the current (REF4) and the target (REF2) horizontal resolutions. In this technical document, we use the namelist parameters names without further explanation of their meaning. The details may be found on the official ALADIN webpages http://www.umr-cnrm.fr/gmapdoc in the Dynamics section of the Specific documentation.

Table 1: Reference experiments setting.

Name	Δx	Δt	Time scheme	Hor.diffusion
REF4	4.7 km	180 s	PC, NSITER=1	slhd1
REF2	2.325 km	90 s	PC, NSITER=1	slhd1

Here "PC" means the following setting for the time scheme:

LPC_FULL=T	LSETTLS=F	LNESC=T
LPC_CHEAP=T	LSETTLST=T	LNESCT=F
	LSETTLSV=T	LNESCV=F

Hence, for the trajectory search the SETTLS scheme is applied in both, the horizontal and the vertical direction, while the iterative centered implicit scheme is applied with NESC (Non-Extrapolating SCheme) method on non-linear terms. Further, "slhd1" means the following setting for the horizontal diffusion:

REXPDH=2.	RDAMPDIV=1.	LSLHD_OLD=F
RRDXTAU=123.	RDAMPDIVS=10.	LSLHD_GFL=T

SDRED=1.	ZSLHDP1=1.7	LSLHD_T=T
SLEVDH=0.1	ZSLHDP3=0.6	LSLHD_W=T
SLEVDHS=1.	RDAMPPD=5.	LSLHD_SPD=T
SLHDEPSH=0.016	RDAMPQ=0.	LSLHD_SVD=T
SLHDEPSV=0.	RDAMPT=1.	YX_NL%LSLHD=T
SLHDKMAX=6.	RDAMPVD=1.	for X=L,I,Q,TKE
SLHDKMIN=-0.6	RDAMPVDS=15.	
SLHDA0=0.25	RDAMPVOR=1.	
SLHDB=4.	RDAMPVORS=10.	
SLHDD00=6.5E-05		

In the current operational application, we use only two iterations of the algorithm for SL trajectory search (NITMP=2). For reasons explained in a separate document [10] we decided to increase the number of iterations for this algorithm to 4 (NITMP=4). The other dynamics options are set as specified at the end of this document in Table 8.

As a diagnostic tool, we first check that the time evolution of the spectral norms of prognostic variables is smooth without big jumps which would question the achieved stability of the experiments; results are not shown here. Second, we study the simulated kinetic energy spectra which provide a useful diagnostic tool for quantifying the model's resolving capability. Kinetic energy spectra may illustrate some of the issues affecting the resolution capabilities of models arising from the choice of spatial grid staggering, integration schemes and their implicit and explicit filters. The spectral kinetic energy budget for various vertical levels is computed as a function of the total horizontal wavenumber. We show -3 and $-5/3$ slopes for canonical atmospheric kinetic energy spectra according to [9] as theoretical limits.
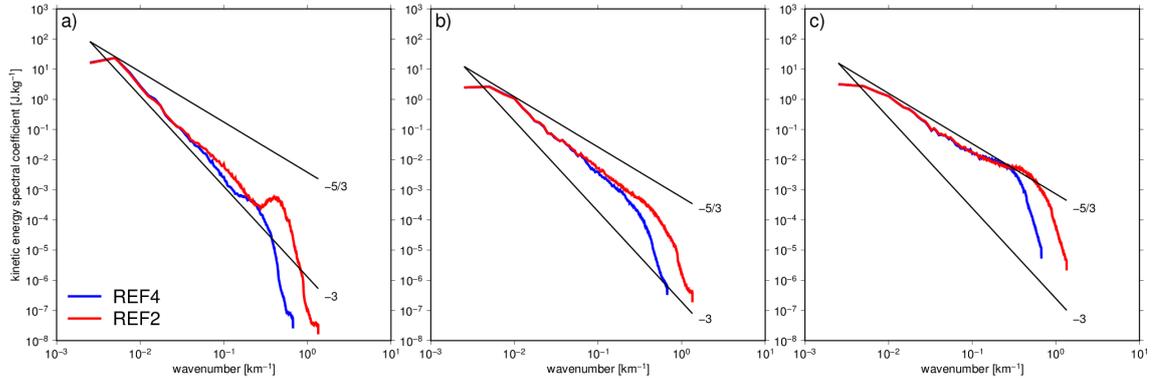

Figure 2: Spectrum of kinetic energy for the reference experiments on 4.7km and 2.325km horizontal resolutions. Diagnostic calculated after 12 hours of integration, at a) 20th, b) 40th and c) 80th model level.

We find that the lack of dissipation at higher model levels leads to energy accumulation in higher wave-numbers for the run with the new resolution REF2 which was not present in coarser resolution run REF4 (or it was only weak); see Figure 2a. We would like to find a setting in the target horizontal resolution with kinetic energy spectra not showing this feature. Middle and low model levels have smooth kinetic energy spectra in both cases; see Fig. 2b,c.

5

3.2 Spectral diffusion strength

Following experiments are run on the target horizontal resolution of $2.325\,km$. The first set of experiments is summarized in Table 2 and it shows that the problem can not be solved by changing the spectral diffusion strength represented by RRDXTAU. We show for comparison the results when no horizontal diffusion is applied and results with only spectral diffusion applied as in the Météo France operational setting of AROME at 1.3km horizontal resolution. The latter setting is denoted "spdif" and it is realized through the following setting:

REXPDH=4.	RDAMPX=20. for all X	LSLHD_OLD=F
RRDXTAU=123.	RDAMPHDS=1.	LSLHD_GFL=T
SDRED=1.	RDAMPXS=0.	LSLHD_X=F
SLEVDH=1.	for all X $\neq$ HD	for all X $\neq$ GFL
SLEVDHS=0.25	SLHDA0=0.25	YX_NL%LSLHD=T
SLHDEPSH=0.08	SLHDB=4.	for X=I,L,R,S
SLHDEPSV=0.	SLHDD00=6.5E-05	
SLHDKMAX=6.	ZSLHDP1=1.7	
SLHDKMIN=0.	ZSLHDP3=0.6	

Table 2: Experiments setting: spectral diffusion strength.

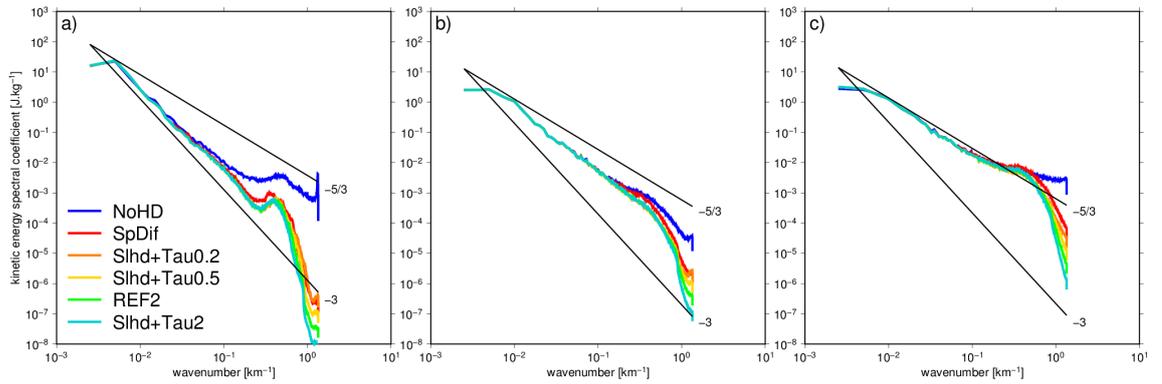| Name	Δt	Time scheme	Hor.diffusion
NoHD	$90\,s$	PC, NSITER=1	no horizontal diffusion
SpDif	$90\,s$	PC, NSITER=1	spdif
Slhd+Tau0.2	$90\,s$	PC, NSITER=1	slhd1 + RRDXTAU=24.6
Slhd+Tau0.5	$90\,s$	PC, NSITER=1	slhd1 + RRDXTAU=61.5
REF2	$90\,s$	PC, NSITER=1	slhd1 + RRDXTAU=123
Slhd+Tau2	$90\,s$	PC, NSITER=1	slhd1 + RRDXTAU=246

Figure 3: As Figure 2, but for different strength of spectral diffusion used with SLHD, without any horizontal diffusion applied, and with spectral diffusion set as in ALADIN-France operational run (spdif); experiments listed in Table 2.

We see that except for the experiment without horizontal diffusion applied, where much

more energy is accumulated in high wave-numbers throughout the whole vertical extent of the domain, the kinetic energy spectra look very similar. The spdif setting shows less damping of short waves, while the effect of RRDXTAU setting is manifested only at the end of spectra as well, throughout the whole domain.

3.3   Number of PC iterations (NSITER)

We ask the question if more precision and enhanced stability brought by one additional iteration of the iterative centered implicit scheme could help to get rid of the generated noise. To get an answer we run experiments with two iterations (correctors) and different time steps as described in Table 3.

Table 3: Experiments setting: two iterations of PC.

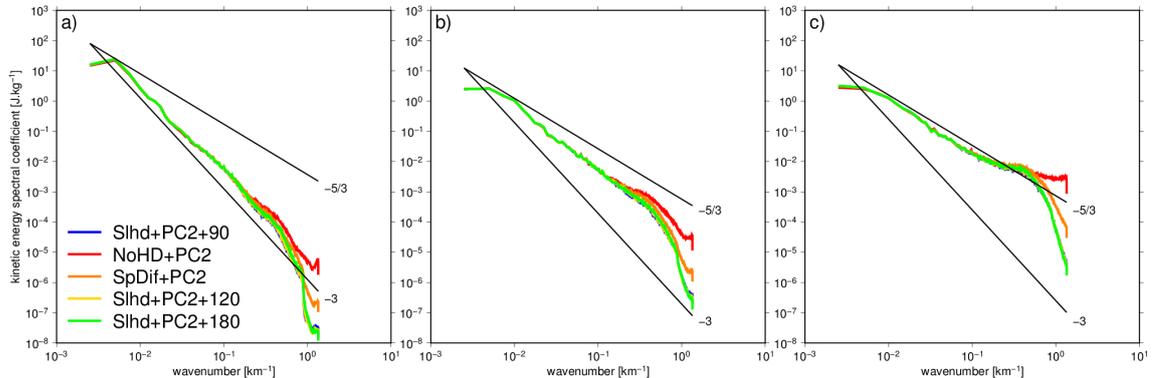| Name	Δt	Time scheme	Hor.diffusion
Slhd+PC2+90	$90\,s$	PC, NSITER=2	slhd1
NoHD+PC2	$90\,s$	PC, NSITER=2	no horizontal diffusion
SpDif+PC2	$90\,s$	PC, NSITER=2	spdif
Slhd+PC2+120	$120\,s$	PC, NSITER=2	slhd1
Slhd+PC2+180	$180\,s$	PC, NSITER=2	slhd1

Figure 4: As Figure 2, but for different time steps and horizontal diffusion settings with two iterations of PC; experiments listed in Table 3.

Here no apparent problems are seen unless the diffusion is switched off. The experiment with Météo France setting (Spdif+PC2) retains more energy in very short wavelengths than all experiments with "slhd1". Moreover, the lack of horizontal diffusion in NoHD+PC2 generates noise in pressure departure field as shown in Figure 7. The spectrum of the square of pressure departure depicted in Figure 5 shows that for all choices the pressure departure field suffers from noisy patterns and the solution depends on many aspects. Different experiments even do not agree on longwave solutions.

Not surprisingly, Slhd+PC2+180 is the least expensive experiment as we show in Appendix, but the time step is heavily exaggerated resulting in noisy fields with spectral norms oscillating between predictor and corrector values as illustrated in Figure 7. But

even with the extremely exaggerated time step, the experiment is running for 24 hours without crashing.
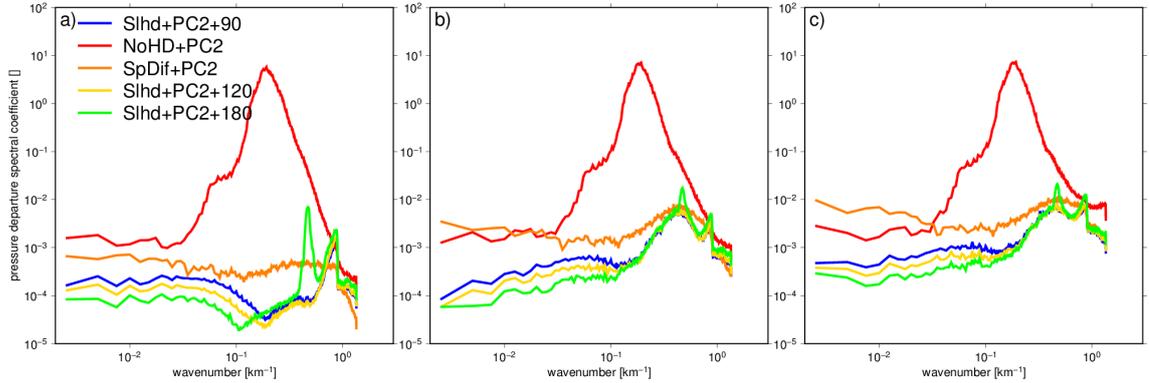

Figure 5: Spectrum of the square of pressure departure for different timesteps and horizontal diffusion settings with two iterations of PC. Diagnostic calculated after 12 hours of integration at a) 20th, b) 40th and c) 80th model level.

We check the stability on spectral norms evolution (saved every fifth timestep for all substeps, predictor and correctors). Another indication of stability is the presence or absence of noise in the pressure departure field. The experiment Slhd+PC2+120 does not show signs of instability in these tests as seen in Figure 7. But we may see an increase in the occurrences of "SMILAG TRAJECTORY UNDERGROUND" messages which means that there is a problem with too strong vertical velocity close to the ground. **We will hence stick on shorter timestep with only one iteration in PC scheme (NSITER=1).**

3.4 Time step

Not surprisingly, shorter time step could help to get rid of the noise as well:
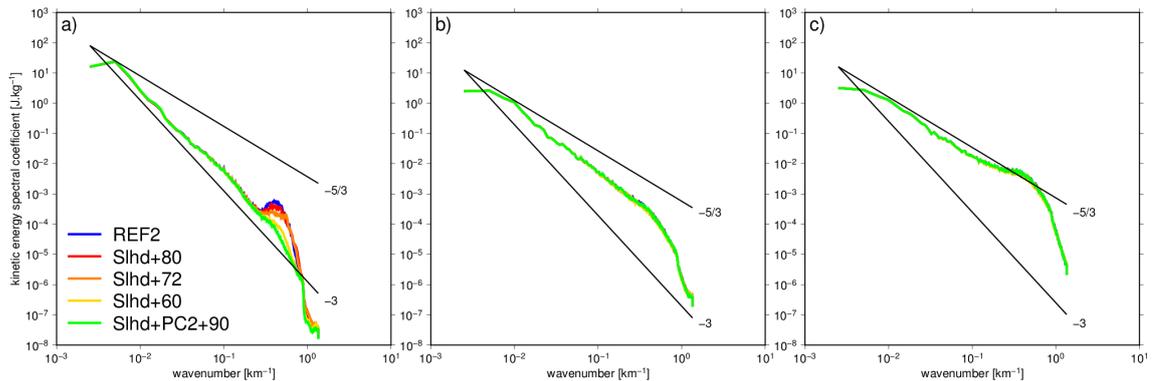

Figure 6: As Figure 2, but for different timesteps used; experiments listed in Table 4.

Here the shortening of the time step to 60s seems to solve the problem, but the solution is expensive. Compare the lumping CPU times needed in Table 11.
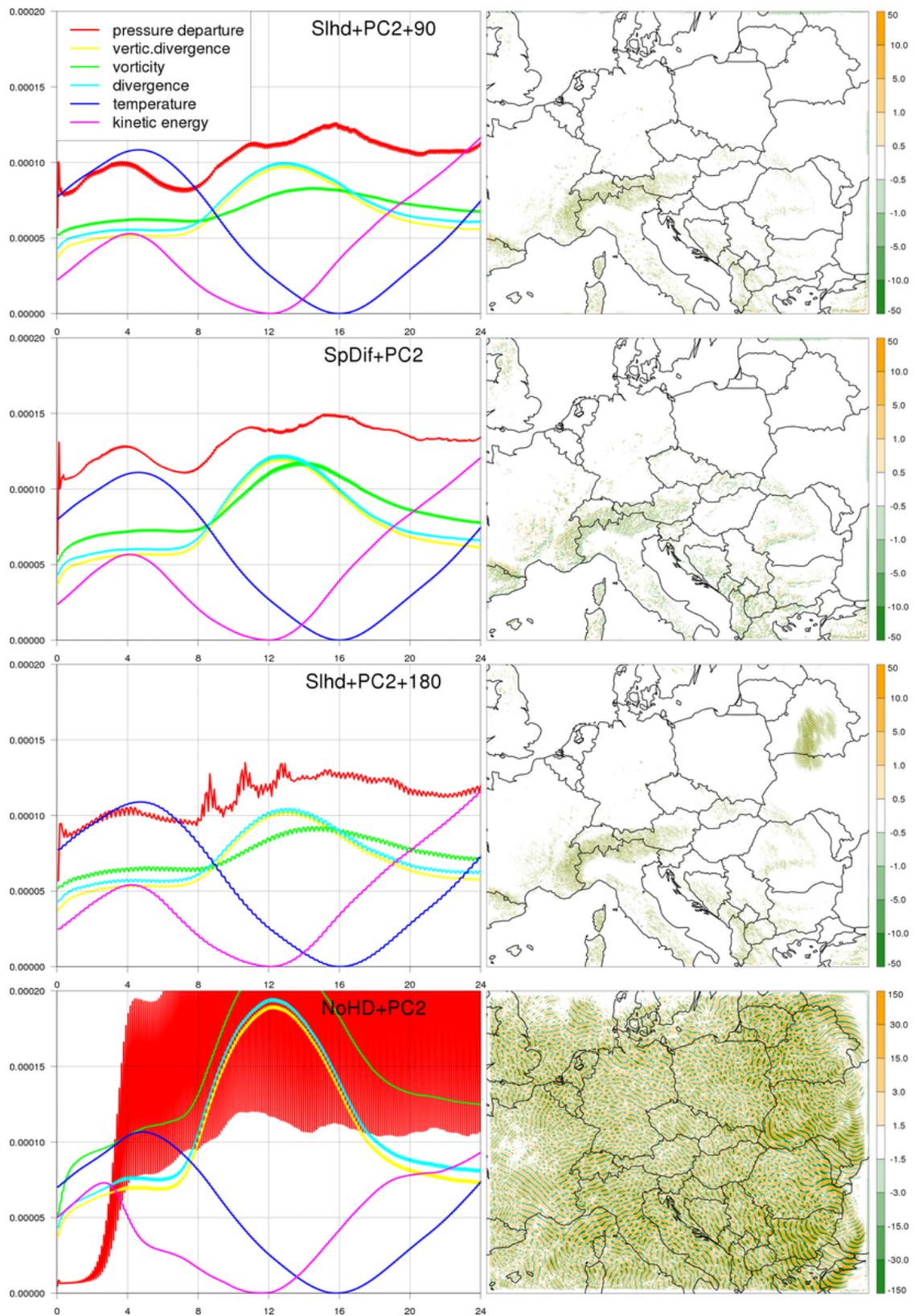
8

Figure 7: Time evolution of the spectral norms for various prognostic variables (left) and the pressure departure field on 20th model level after 12 hours of integration (right) for different experiments with two corrector steps.

Table 4: Experiments setting: time step.

Name	Δt	Time scheme	Hor.diffusion
Slhd+80	$80\,s$	PC, NSITER=1	slhd1
Slhd+72	$72\,s$	PC, NSITER=1	slhd1
Slhd+60	$60\,s$	PC, NSITER=1	slhd1

3.5 Enhanced spectral horizontal diffusion

As an alternative, we may try to enhance the reduced spectral horizontal diffusion when SLHD is applied through modified SDRED parameter.

Table 5: Experiments setting: reduced spectral diffusion parameter SDRED.

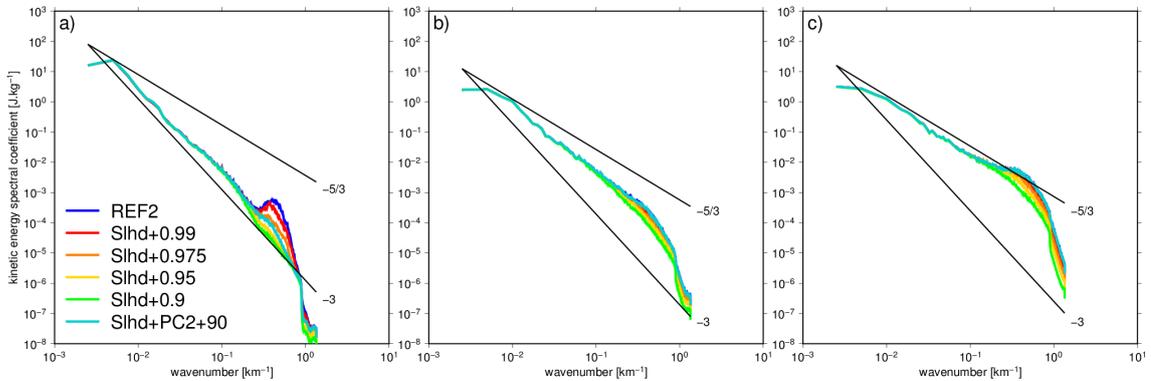| Name	$\Delta t[s]$	Time scheme	Hor.diffusion
REF2	$90\,s$	PC, NSITER=1	slhd1
Slhd+0.99	$90\,s$	PC, NSITER=1	slhd1 + SDRED=0.99
Slhd+0.975	$90\,s$	PC, NSITER=1	slhd1 + SDRED=0.975
Slhd+0.95	$90\,s$	PC, NSITER=1	slhd1 + SDRED=0.95
Slhd+0.9	$90\,s$	PC, NSITER=1	slhd1 + SDRED=0.9

Figure 8: Spectrum of kinetic energy for different values of SDRED used. Diagnostic calculated after 12 hours of integration, at a) 20th, b) 40th and c) 80th model level.

The effect of a value of SDRED < 1 is that the spectral horizontal diffusion is applied in the whole vertical extent of the domain, even if just a small portion (depending on SDRED). We may see the effect at lower model levels (40th, 80th) where it is not needed. Conceptually, we prefer to avoid such solution. **Hence we keep SDRED=1.**

We may also extend the region in which the reduced spectral diffusion is applied from the top of the domain through SLEVDH parameter. Since resulting vertical profile of horizontal diffusion coefficient is multiplied by RRDXTAU, we show the vertical profile of the parameter PDILEV_SLD*RRDXTAU for several experiments and then we show

the kinetic energy spectra of these experiments. Parameters SLEVDH and SLEVDH3 are needed (and SDRED; we have SDRED=1 here) to calculate PDILEV_SLD.

Table 6: Experiments setting: reduced spectral diffusion parameter SLEVDH.

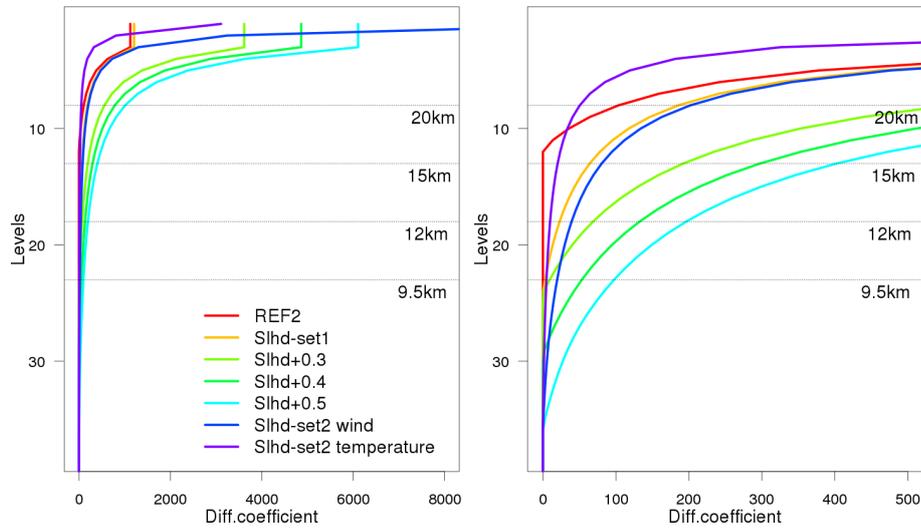| Name	$\Delta t[s]$	Time scheme	Hor.diffusion
REF2	$90\,s$	PC, NSITER=1	RRDXTAU=123., SLEVDH=0.1
Slhd+0.2	$90\,s$	PC, NSITER=1	RRDXTAU=123., SLEVDH=0.2
Slhd+0.3	$90\,s$	PC, NSITER=1	RRDXTAU=123., SLEVDH=0.3
Slhd+0.4	$90\,s$	PC, NSITER=1	RRDXTAU=123., SLEVDH=0.4
Slhd+0.5	$90\,s$	PC, NSITER=1	RRDXTAU=123., SLEVDH=0.5

Figure 9: Vertical profile of the diffusion coefficient for the reduced spectral diffusion, the part not depending on the horizontal wave number. The zoom on small values is on the right panel.
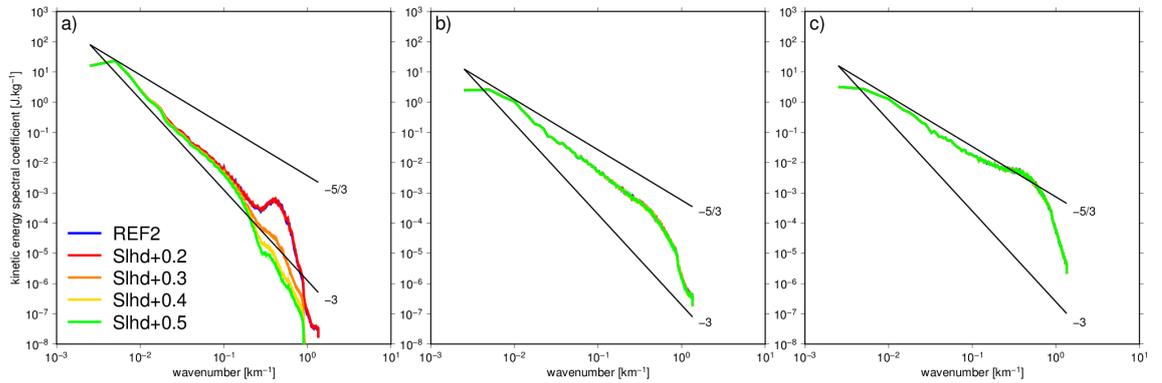

Figure 10: Spectrum of kinetic energy for different SLEVDH values. Diagnostic calculated after 12 hours of integration, at a) 20th, b) 40th and c) 80th model level.

The problem of cumulated energy disappears as soon as SLEVDH $\geq$ 0.3. But the diffusion

seems to be too strong in higher atmosphere in these cases. Hence we try to make the diffusion weaker by reducing RRDXTAU in Slhd-set1, or by introducing weaker damping separately for temperature and relative humidity, and separately for vorticity, divergence and pressure departure in Slhd-set2. The SLHD setting denoted "slhd2" used for Slhd-set2 differs from "slhd1" in the following parameters:

SLEVDH=0.5	RDAMPDIV=5.	RDAMPT =20.
	RDAMPVOR=5.	RDAMPQ =20.
	RDAMPPD =5.	RDAMPVD=20.

while values of the following parameters are kept:

RRDXTAU=123.	RDAMPPD=5.	RDAMPDIVS=10.
		RDAMPVORS=10.
		RDAMPVDS=15.

Table 7: Experiments setting: three alternatives for SLHD.

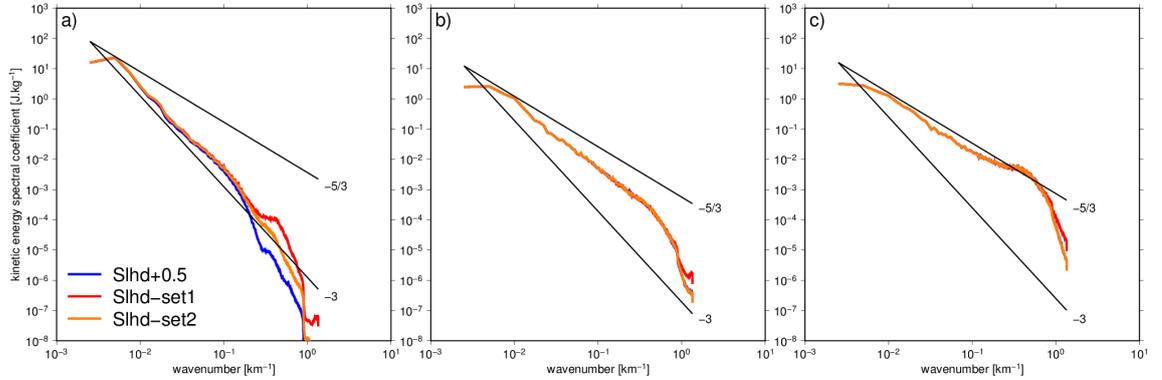| Name	$\Delta t[s]$	Time scheme	Hor.diffusion
Slhd+0.5	$90\,s$	PC, NSITER=1	slhd1 + RRDXTAU=123., SLEVDH=0.5
Slhd-set1	$90\,s$	PC, NSITER=1	slhd1 + RRDXTAU=41., SLEVDH=0.3
Slhd-set2	$90\,s$	PC, NSITER=1	slhd2 + RRDXTAU=123., SLEVDH=0.5

Figure 11: Spectrum of kinetic energy for several alternative SLHD settings listed in Table 7. Diagnostic calculated after 12 hours of integration, at a) 20th, b) 40th and c) 80th model level.

In Slhd-set2 the spectral diffusion is applied in boarder zone of atmosphere then originally, starting from approximately 35th model level and going to the top of the atmosphere. The diffusion coefficient for temperature and vertical divergence is slightly weakened while on the other hand, the diffusion coefficient for wind (divergence, vorticity) is slightly amplified as can be seen in Fig. 9. We may see that the kinetic energy spectra at 20th model level is smoothest for Slhd-set2 while there is no additional loss of energy compared to the original setting REF2 in lower model levels. **We consider Slhd-set2 setting as a good candidate for the target operational application.**
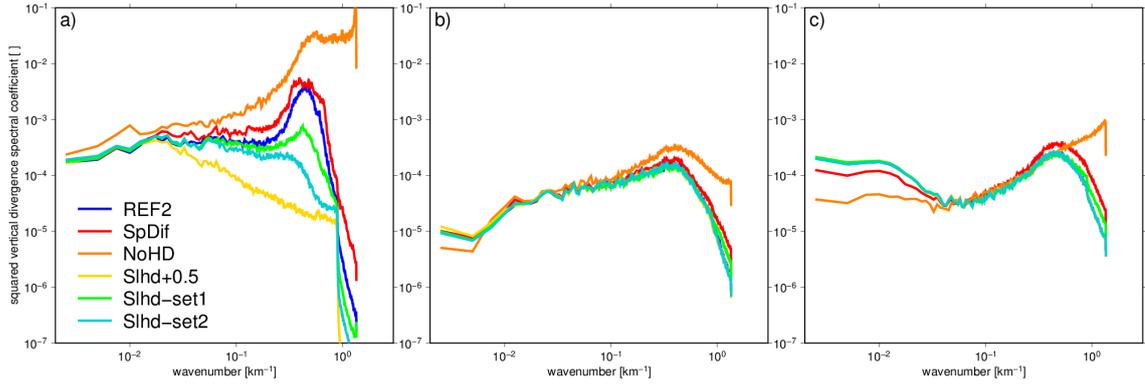
12

Figure 12: Spectrum of square of vertical divergence for different vertical profiles of the diffusion coefficient for the reduced spectral diffusion, after 12 hours of integration. Diagnostic calculated after 12 hours of integration, at a) 20th, b) 40th and c) 80th model level.

3.6 Vertical discretization

In the ALADIN System, the hybrid pressure based terrain following vertical coordinate is used, in the nonhydrostatic version designed by Laprise. In the current operational application with hydrostatic dynamics the vertical discretization is using finite element method implemented according to [11]. For nonhydrostatic dynamics, the appropriate finite element method was developed in [12] and implemented in the ALADIN System for general accuracy order. Unfortunately, for both methods we observe a spurious mode in the enthalpy field close to the domain top where the vertical resolution is coarser. An illustration with the diagnostic tool called DDH (Diagnostics in Horizontal Domains) is in Figure 13. Hence for the target nonhydrostatic operational application, finite difference method is used for vertical discretization, having generally only first order accuracy but without spurious mode in the enthalpy field.
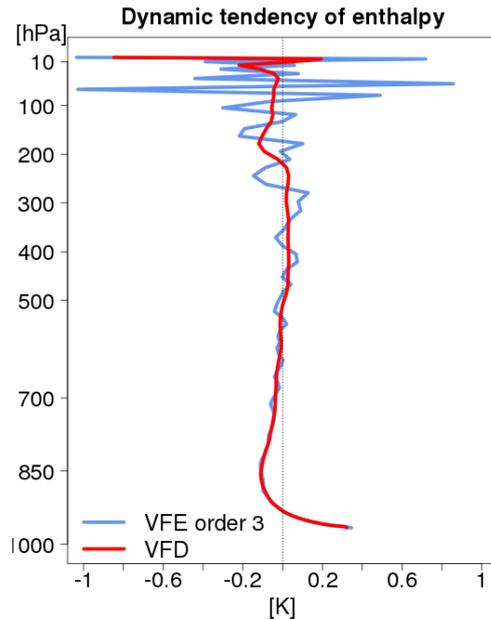

Figure 13: The dynamic tendency of enthalpy averaged horizontally and in time in hydrostatic experiments with different discretizations of vertical integrals: VFE - finite element, VFD - finite difference method.

4 Long runs

We run longer period of experiments for several settings, from 3 January 2017 to 16 January 2017, integration for 72 hours once per day starting from 00 UTC. During this

13

period, the Czech territory was hit with strong westerly winds, while almost no humidity and rain were present. Hence physical parameterizations are not very active and dynamics plays essential role here. These experiments were run in a BlendVar cycle as the Czech operational run. The results for temperature at 250 hPa are shown in Figure 14 while the other characteristics were rather neutral.

We may see that there is a considerable gain in RMSE and bias when Slhd-set2 is used compared to other experiments. The dynamics setting of Slhd-set2 has the best performance we were able to get and was tested in a parallel suite. See Section 6 for an illustration of results obtained.
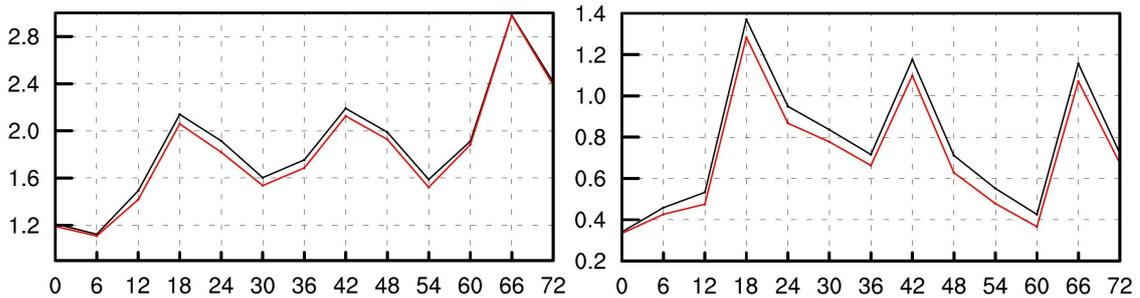

Figure 14: RMSE and BIAS for temperature at 250 hPa for the serie of experiments 3-16/1/2017. Black color is as in Slhd-set1, red color as in Slhd-set2.

We checked the shape of some meteorological fields for the executed experiments and found overall very similar results. For example, the precipitation cumulated for 3 hours from 15 UTC to 18 UTC, 8 June 2016, are similar for all experiments. We show only several of them in Figure 15. We may see here that the shape of precipitation is preserved after the horizontal resolution change, just the granulation is finer. This indicates that the ALADIN/ALARO model performance has seamless features.
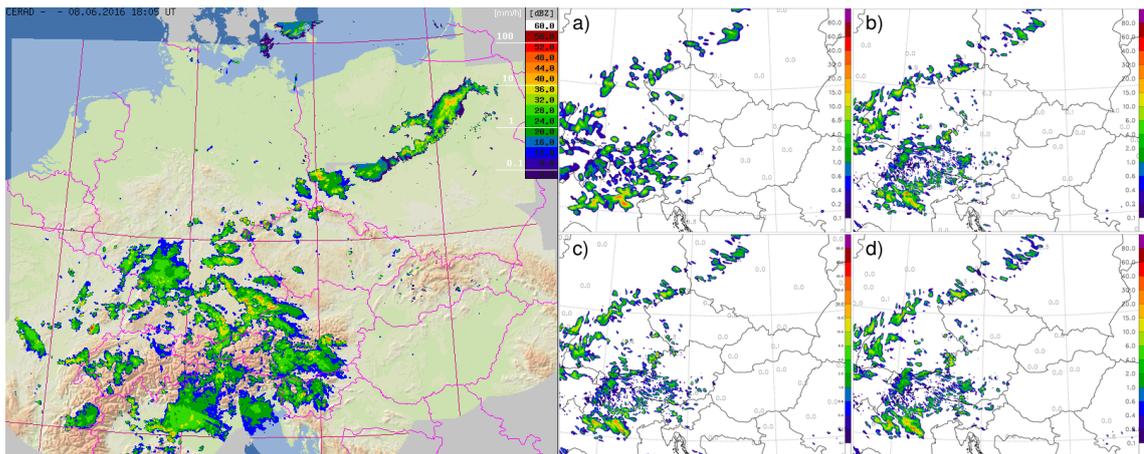

Figure 15: Precipitation on 8 June 2016 18 UTC. Left panel: Central European radar network (CERAD) composite shows instantaneous reflectivity. Right panels: Precipitation cumulated for 1 hour, forecast from the experiment a) REF4, b) REF2, c) Slhd-set1, d) Slhd-set2. Maxima in the domain are indicated.

14

5 Recommended options

Considering all previous results and summarizing them, we get the dynamical options as follows:

TSTEP=90.	REXPDH=2.	SLHDA0=0.25
NSITER=1	RRDXTAU=123.	SLHDB=4.
LPC_FULL=T	SDRED=1.	SLHDD00=6.5E-05
LPC_CHEAP=T	SLEVDH=0.5	SLHDEPSH=0.016
LSETTLS=F	SLEVDHS=1.	SLHDEPSV=0.
LSETTLST=T	RDAMPDIV=5.	SLHDKMAX=6.
LSETTLSV=T	RDAMPVOR=5.	SLHDKMIN=-0.6
LNESC=T	RDAMPPD=5.	LSLHD_OLD=F
LNESCT=F	RDAMPT=20.	LSLHD_GFL=T
LNESCV=F	RDAMPQ=20.	LSLHD_T=T
NITMP=4	RDAMPVD=20.	LSLHD_W=T
	RDAMPDIVS=10.	LSLHD_SPD=T
	RDAMPVORS=10.	LSLHD_SVD=T
	RDAMPVDS=15.	YX_NL%LSLHD=T
	ZSLHDP1=1.7	for X=L,I,Q,TKE
	ZSLHDP3=0.6	YX_NL%LPC=T
		for all X with
		YX_NL%LADV=T

This setting may be used as it is in the official ALADIN cycle CY43t2, while some alteration may be needed for other model cycles. We recommend these options to be used in the target operational application of the ALADIN System at CHMI at 2.325km resolution with nonhydrostatic fully elastic equations.

The other dynamics parameters are set in all nonhydrostatic experiments according to Table 8.

Further tuning is being done in the other model parts as physical parameterizations, surface characteristics and data assimilation cycle, which is expected to bring more improvements into the results of the new operational application of the ALADIN System at CHMI. These considerations are out of the scope of this document.

6 Parallel suites comparison

A parallel suite is being run with the new setting on the target horizontal resolution of 2.325km whose results are continuously compared to the current operational results to make sure that the overall behaviour is satisfactory. We show a nice example of the cloudiness which is formed much more realistically in the target resolution run using nonhydrostatic equations than with the previous setting with hydrostatic primitive equations

at 4.7km; see Fig. 17. Such formation of clouds is typical for leeward side of mountains which represent an obstacle in a flow. The case is from 12 February 2019, forecast valid for 11UTC.

Table 8: Dynamical parameters used in all experiments mentioned.

NH dynamics	LNHDYN=T (LNHEE=T, LNHQE=F for CY46 and higher)
NH variables	NPDVAR=2, NVDVAR=4, ND4SYS=1, LGWADV=T, LRDBBC=F
Advection	LSLAG=T
SL interpolations	NXLAG=3 for X=T,V,W,SPD,SVD, LQMX=F for all X (default values plus X=HW,HT,P)
Time scheme	LTWOTL=T
SI reference state	SIPR=90000., SITR=350., SITRA=100.
Decentering	VESL=0., XIDT=0.
Vertical discretization	LVERTFE=F, NDLNPR=1

Appendix: CPU time and effectivity

Reference

We compare the efficiency of hydrostatic versus nonhydrostatic runs of the AL-ADIN/ALARO/AROME numerical weather prediction system. Furthermore, we compare the CPU time needed for two time schemes: SETTLS (Stable Extrapolation Two-Time Level Scheme according to [7]) and PC (iterative centered implicit scheme with one iteration according to [1] without recomputation of SL trajectories). The experiments are run on the current and the target horizontal resolutions, otherwise with the current operational setting, first in adiabatic regime and then with full ALARO physics (version 1). We use various numbers of nodes of the Czech NEC HPC based on Intel Broadwell technology in mixed MPI/OpenMP mode and measure the lumping CPU time.

We use 180s time step for 4.7km horizontal resolution, and 90s time step for 2.325km horizontal resolution, independently from other choices. For adiabatic runs we omit here to write to files completely and do not calculate spectral norms. The relative humidity is set to zero everywhere and treated as spectral, but it is not changed by physics. We use four iterations of the algorithm for SL trajectory search (NITMP=4).
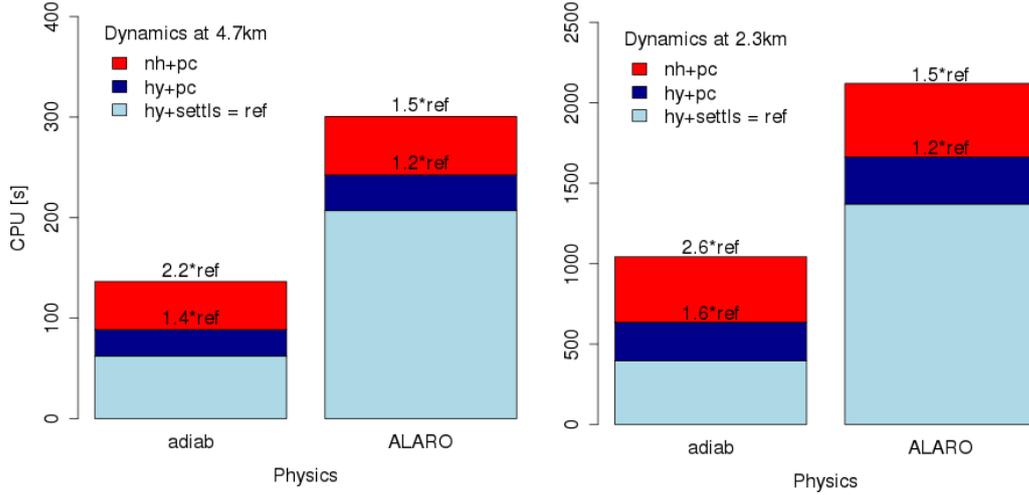
Figure 16: The average (over number of nodes used) lumping CPU time needed for one integration for 24 hours.

The results are summarized in Table 9 and 10 and the average results for each horizontal resolution in adiabatic and full ALARO physics regimes are illustrated in Figure 16.

Table 9: CPU time needed for one integration for 24 hours.

$\Delta x = 4.7 km$ — CPU [s] + Percentage

Time scheme	Physics	Dyn	NODES					
			24		48		72	
SETTLS	adiab	hy	59	100%	35	100%	31	100%
PC	adiab	hy	85	144%	51	148%	41	132%
PC	adiab	nh	136	231%	77	220%	60	194%
SETTLS	ALARO	hy	203	100%	118	100%	93	100%
PC	ALARO	hy	237	117%	140	119%	108	116%
PC	ALARO	nh	295	145%	172	146%	134	144%

Table 10: CPU time needed for one integration for 24 hours.

$\Delta x = 2.325 km$ — CPU [s] + Percentage

Time scheme	Physics	Dyn	NODES					
			24		48		72	
SETTLS	adiab	hy	410	100%	225	100%	159	100%
PC	adiab	hy	671	164%	360	160%	241	152%
PC	adiab	nh	1069	261%	592	263%	425	267%
SETTLS	ALARO	hy	1439	100%	764	100%	538	100%
PC	ALARO	hy	1750	122%	927	121%	649	121%
PC	ALARO	nh	2213	154%	1179	154%	848	158%

We may see that the nonhydrostatic dynamics is more efficient in coarser resolution while in higher resolution there is a bigger increase in CPU time needed compared to hydrostatic dynamics. When adiabatic runs are compared, nonhydrostatic dynamics needs about 2-3 times the CPU used by hydrostatic dynamics, while in the full model run with ALARO physics this number decreases to approximately 1.5.

The PC scheme without recomputation of SL trajectories (LPC_CHEAP=T, NSITER=1) needs much less then two times the CPU time used by SETTLS (one step) scheme. It uses only about 20% in addition in the full model with ALARO physics.

Number of PC iterations (NSITER)

We compare the CPU time usage of experiments from Table 3 with the CPU time needed for the reference experiments. We run the 24 hours integration for each experiment on 45 nodes of the Czech NEC HPC in the OpenMP mode (8x3). The lumping CPU times are summarized in Table 11.

It follows that Slhd+PC2+120 is the most effective choice among all experiments giving meteorologically meaningful results. For reasons explained in Section 3.3 we prefer shorter time step with only one additional iteration of the PC scheme.

Table 11: The lumping CPU times measured and compared to reference experiments.

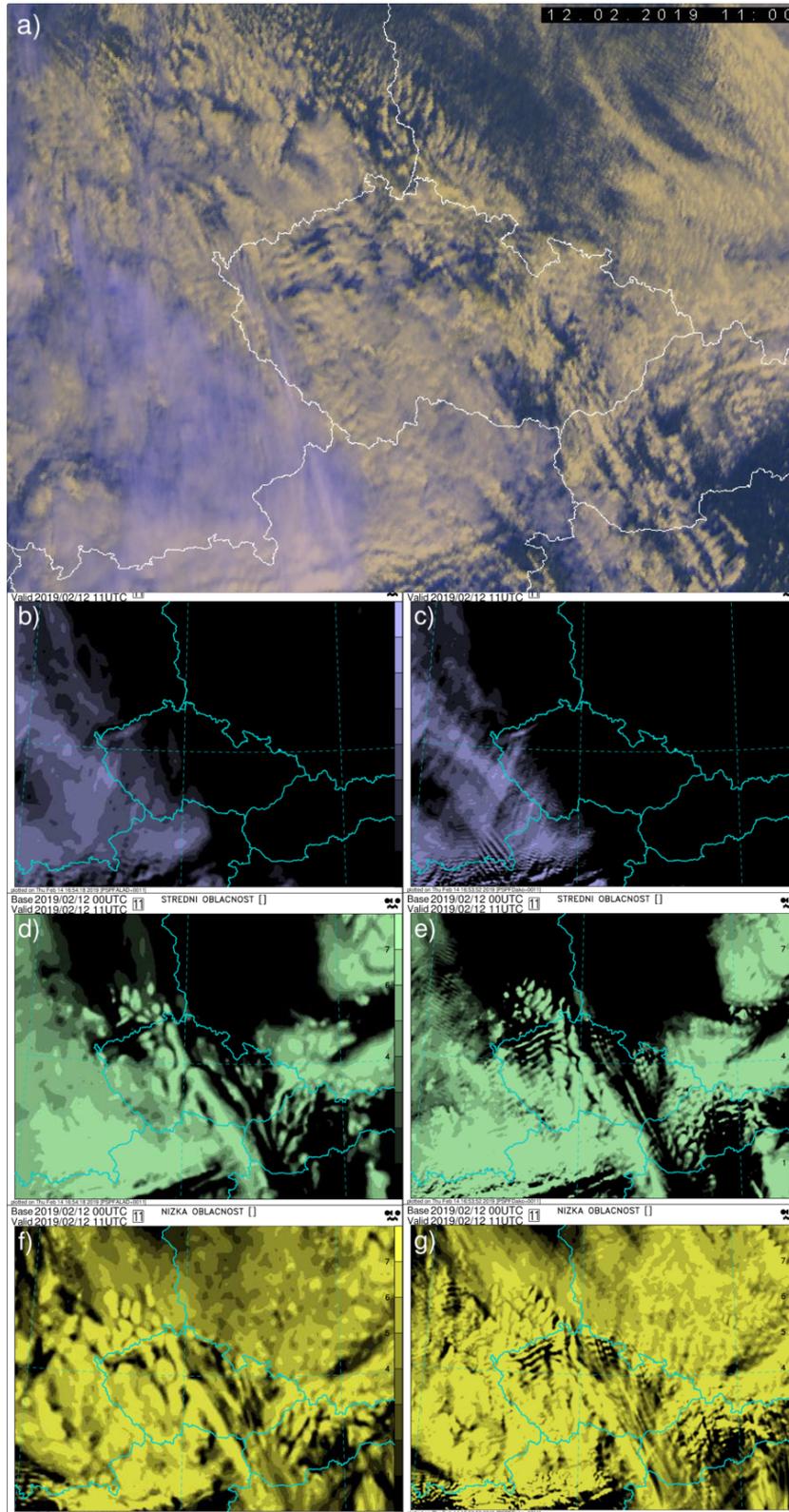| Name	$\Delta t[s]$	Time scheme	CPU[s]	Percentage
REF4	180	PC,NSITER=1	187	
REF2	90	PC,NSITER=1	1245	670% of REF4
Slhd+80	80	PC,NSITER=1	1351	108% of REF2
Slhd+72	72	PC,NSITER=1	1479	119% of REF2
Slhd+60	60	PC,NSITER=1	1767	142% of REF2
Slhd+PC2+90	90	PC,NSITER=2	1455	117% of REF2
Slhd+PC2+100	100	PC,NSITER=2	1325	106% of REF2
Slhd+PC2+120	120	PC,NSITER=2	1114	89% of REF2
Slhd+PC2+180	180	PC,NSITER=2	816	66% of REF2

Figure 17: Cloudiness for 12 February 2019 at 11 UTC a) observed by geostationary satellite METEOSAT (Vis-IR channel) and predicted with 4.7km operational version of ALARO (b,d,f); and with 2.325km parallel suite of ALARO (c,e,g), both integrated from 12 February 2019 00UTC. From top to bottom - high cloudiness, middle level cloudiness, low cloudiness.

References

[1] P. Bénard. Stability of semi-implicit and iterative centered-implicit time discretizations for various equation systems used in NWP. *Mon. Weather Rev.*, 131(10):2479–2491, 2003.

[2] P. Bénard, J. Vivoda, J. Mašek, P. Smolíková, K. Yessad, Ch. Smith, R. Brožková, and J. F. Geleyn. Dynamical kernel of the Aladin–NH spectral limited-area model: Revised formulation and sensitivity experiments. *Q. J. R. Meteorol. Soc.*, 136(646):155–169, 2010.

[3] P. Courtier, C. Freydier, J.-F. Geleyn, F. Rabier, and M. Rochas. The ARPEGE project at Météo-France. *Proceedings of 1991 ECMWF Seminar on Numerical Methods in Atmospheric Models*, ECMWF, Reading, UK:193–231, 1991.

[4] P. Courtier and J.-F. Geleyn. A global numerical weather prediction model with variable resolution: Application to the shallow model equations. *Q. J. R. Meteorol. Soc.*, 114:1321–1346, 1988.

[5] L. Bengtsson et al. The HARMONIE-AROME model configuration in the ALADIN-HIRLAM NWP system. *Mon. Weather Rev.*, 145:1919–1935, 2017.

[6] P. Termonia et al. The ALADIN System and its canonical model configurations AROME CY41T1 and ALARO CY40T1. *Geosci. Model Dev.*, 11:257–281, 2018.

[7] M. Hortal. The development and testing of a new two-time-level semi-lagrangian scheme (SETTLS) in the ECMWF forecast model. *Q. J. R. Meteorol. Soc.*, 128(583):1671–1687, 2002.

[8] F. Váňa, P. Bénard, J.-F. Geleyn, A. Simon, and Y. Seity. Semi-Lagrangian advection scheme with controlled damping: An alternative to nonlinear horizontal diffusion in a numerical weather prediction model. *Q. J. R. Meteorol. Soc.*, 134:523–537, 2008.

[9] William C. Skamarock, Sang-Hun Park, Joseph B. Klemp, and Chris Snyder. Atmospheric kinetic energy spectra from global high-resolution nonhydrostatic simulations. *J. Atmos. Sci.*, 71(11):4369–4381, 2014.

[10] P. Smolíková and A. Craciun. The trajectory search in the SL computations. *RC LACE report*, 2018.

[11] A. Untch and M. Hortal. A finite-element scheme for the vertical discretization of the semi-Lagrangian version of the ECMWF forecast model. *Q. J. R. Meteorol. Soc.*, 130(599):1505–1530, 2004.

[12] J. Vivoda, P. Smolíková, and J. Simarro. Finite elements used in the vertical discretization of the fully compressible core of the ALADIN System. *Mon. Weather Rev.*, 146(10):3293–3310, 2018.